Mathematical Modelling and Data-Driven Protection Algorithm for Fault Current Calculation in Bipolar Medium Voltage Multi-Terminal DC Networks

Zeeshan Haider, Arif Mehdi, Gwang-Su Shin, S Jarjees Ul Hassan, Chul-Hwan Kim

***Abstract*-- Faults in Medium Voltage Direct Current (MVDC) distribution networks present unique challenges, particularly in systems with bipolar configurations. The critical challenges include the high-speed fault current rise due to low network impedance, making fault interruption difficult, and the complex coordination of protection schemes in multi-terminal configurations. This paper focuses on the calculation of fault currents in a five-terminal bipolar MVDC distribution system, specifically under pole-to-pole (PTP) fault. The branch currents in the MVDC network are computed using mathematical modeling to provide critical data for fault current estimation. This data is utilized to train an artificial neural network (ANN) algorithm for fault location estimation, with 80% of the data dedicated to training, 10% for testing, and 10% for validation. The ANN achieves a RMSE of 0.8090, MAE of 0.3896, and R^2 of 0.9912, significantly outperforming support vector regression (SVR). Further analysis, including noise and parameter deviations, shows that the ANN maintains high accuracy, with R^2 values above 0.97. This confirms the robustness of the proposed method for real-world applications. These results confirm that the proposed ANN-based method offers an accurate and efficient fault location approach for MVDC networks, aiding the development of advanced protection schemes to enhance system reliability and safety.**

***Keywords*: Bipolar MMC, Fault Location, MVDC Distribution, Mathematical Modeling, Pole-to-Pole Fault.**

I. Introduction

In recent years, the world has been transitioning towards renewable energy to meet the energy requirements. Renewable energy's share in primary energy supply is projected to rise from 14% in 2015 to 63% by 2050, with fossil fuels decreasing from 86% to 37% [1]. One of the prime reasons for shifting toward renewable energy resources (RES) is the decline of fossil fuels [2]. However, the intermittent and unpredictable nature of RES introduces challenges, particularly when integrating them with traditional AC systems [3]. Synchronization issues arise due to the fundamental differences between AC and DC systems [4]. In this context, DC transmission and distribution offers an ideal solution by enabling easier and more efficient integration of RES into the grid [5]. Due to their flexible control capabilities, improved voltage levels, and increased transmission and distribution capacity, Modular Multilevel Converter (MMC)-based multi-terminal (MT) HVDC and MVDC systems have become widely used in applications such as RES integration, urban power distribution, and offshore wind farms [6]. There has been a lot of interest in switching to DC distribution systems because of their benefits over conventional AC systems [7]. MVDC systems are being used more and more for applications where minimizing power losses and simplifying power flow control are essential [8].

However, despite these advantages, the protection and fault detection mechanisms in MVDC systems remain a significant challenge. Unlike AC systems, where fault detection is well established, DC systems lack natural zero-crossings, making it more difficult to detect and isolate faults quickly [9]. This is especially crucial in bipolar MVDC systems, where a fault can either occur between the two poles (PTP fault) or between a pole and ground (PTG fault), leading to different impacts on the system's operation [10].

Analyzing the fault response is essential for a DC network based on an MMC to protect power semiconductors, like IGBTs, from possible harm caused by overcurrent or overvoltage situations [11]. Whenever a DC fault happens, all MMC capacitors immediately discharge, which causes high currents to flow to the fault location and starts the fault evolution process [12], [13]. This fault current's magnitude is far higher than it would be during normal operation of the DC network [6], [14]. Before the MMC protection controller acts and blocks all submodules (SMs), this period usually lasts up to 10 milliseconds [15].

Thus, effective fault detection and location methods are essential for ensuring the reliability and stability of MVDC distribution networks. Accurate calculation of fault currents is the first step in developing these methods, as it provides critical information for protection schemes and helps determine the characteristics of different types of faults. This information is also fundamental for developing algorithms that can precisely locate faults along the DC distribution line, enabling rapid isolation and restoration of the system.

Various approaches have been proposed in the literature for calculating fault currents and detecting fault locations in

This work was supported by the Korea Institute of Energy Technology Evaluation and Planning (KETEP) and the Ministry of Trade, Industry & Energy (MOTIE) of the Republic of Korea (No. 20225500000110).

The authors are with the Department of Electrical and Computer Engineering, Sungkyunkwan University, Suwon 16419, Republic of Korea

(e-mail: zeeshan776@skku.edu; mehdiarif@skku.edu; shin5565@skku.edu; jarjees@skku.edu; chkim@skku.edu)

Paper submitted to the International Conference on Power Systems Transients (IPST2025) in Guadalajara, Mexico, June 08-12, 2025.

MVDC systems. Extensive calculations have been performed for the MMC and each branch of the system to examine the fault currents caused by capacitor discharging [6], [16], [17]. Some methods focus on analytical models and numerical simulations to predict fault behavior, while others leverage artificial intelligence to identify fault patterns. Numerous studies, such as [18], have extensively analyzed fault currents for monopole configurations using half-bridge MMCs. However, fault current estimations for bipolar full-bridge MMC-based MVDC systems have received little attention. which limits the existing methods in more complex network configurations. This limits the applicability of existing fault detection techniques to more complex network configurations. Despite these efforts, challenges remain in achieving high accuracy and robustness in fault detection, particularly under varying system conditions and noises [19].

Existing literature on fault detection methods, including traveling wave techniques [20], impedance-based strategies [21], and artificial intelligence (AI)-based algorithms [22], has several limitations when applied to full-bridge bipolar MVDC systems. Traveling wave techniques require high sampling rates and extensive sensor deployment, making them impractical for large MVDC systems. Impedance-based strategies are highly sensitive to parameter deviations, leading to inaccuracies under varying system conditions. AI-based algorithms, though promising, rely heavily on simulation data, limiting their real-world applicability. Machine learning methods have recently drawn interest in fault location because of their versatility and capacity to deal with nonlinear data patterns [23]. However, existing methods in the literature primarily rely on simulation-based data for fault location estimation, with no studies found that utilize analytically derived data. Additionally, the current literature predominantly focuses on monopole and half-bridge (HB) topologies, leaving a gap in research for bipolar full-bridge (FB) configurations.

The objective of this paper is to address these challenges by presenting a comprehensive methodology for calculating fault currents in a bipolar MVDC distribution system for PTP faults. The calculated fault currents are then used to develop a fault detection algorithm to enhance the speed and accuracy of fault location. The key contributions of this paper are summarized as:

- Compared to existing approaches this paper derives analytical fault current expressions for bipolar MVDC systems, improving stability and performance of MTDC.
- This algorithm outperforms traditional PTP methods, ensuring faster and more precise fault detection.
- The existing strategies focused on monopolar and HB structure; this scheme effectively handles complex full-bridge (FB) bipolar MTDC fault scenarios.
- The algorithm is validated through extensive MATLAB simulations, proving its robustness across various fault conditions.

The remaining sections of the paper are organized as: Section II addresses the fault response of an MMC and its equivalent circuit. Additionally, the MTDC network's mathematical modeling is shown in Section III. The implementation of a fault location estimation algorithm and fault current calculations are presented in Section IV, and the paper is finally concluded in Section V.

II. Fault Response Modeling for MMC in MVDC Distribution

A. FB-MMC Equivalent Model

A three-phase Modular Multilevel Converter (MMC) is shown in Fig. 1(a), while Fig. 1(b) provides further information on the Full-Bridge Submodule (FBSM). In steady-state operation, the MMC output voltage, Vdc, is kept close to the rated DC grid voltage. Each phase consists of two arms that can be described as an RLC circuit in the early phases of a DC short circuit. These arms have submodules, resistance, and arm inductance.

Short-circuit faults in DC grids can be classified into two main categories: PTG faults and PTP faults. PTP faults have more severe effects on the currents flowing through each MMC for distribution or transmission, as evaluated in [6], [10], [24], although PTG faults are more common. Above all, the analysis concentrates on the Full-Bridge Submodule (FBSM) based MTDC system in the time frame before submodule (SM) blocking, which poses the most significant challenge.

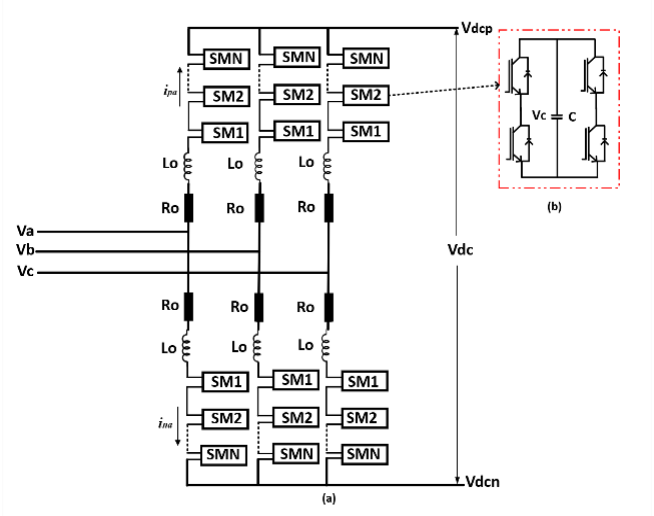

Fig. 1 (a) MMC Equivalent (b) FB-Sub Module

R_0, L_0, and C_0 are arm resistance, arm inductances, and sub-module capacitance respectively. The equivalent of each can be derived using (1)-(3)

$$R_{eq} = \frac{2R_0}{3} \tag{1}$$

$$L_{eq} = \frac{2L_0}{3} \tag{2}$$

$$C_{eq} = \frac{6C_0}{N_{SM}} \tag{3}$$

Where N_{SM} is the number of sub-modules in the arm. In a bipolar system, the equivalent resistance and inductance will be double, and capacitance will be half. The equivalent RLC parameters for the bipolar MMC system are

$$R_e = \frac{4R_0}{3} \quad (4)$$

$$L_e = \frac{4L_0}{3} + L_r \quad (5)$$

$$C_e = \frac{3C_0}{N_{SM}} \quad (6)$$

In (5) L_r is the smooth reactance. To ensure accurate fault current in this calculation, the source current of the MMC is also considered. In [24] modified average value model (MAVM) of the MMC is defined considering the source current. The source current depends upon the control system of the MMC for power power-controlling terminal, the source current is calculated using (7)

$$i_s(t) = \frac{P^*}{u_c(t)} \quad (7)$$

Where P^* is the AC power reference and $u_c(t)$ capacitor voltage. For the voltage control, the source current can be found using (8)

$$i_s(t) = k_{p,U}.\left(U^*_{dc} - u_c(t)\right) + k_{i,U}\int\left(U^*_{dc} - u_c(t)\right)dt \quad (8)$$

Where U^*_{dc} is the DC reference voltage and $k_{p,\,U,}$ and $k_{i,\,U}$ are the proportional gain and integral gain of the DC voltage controller.

B. Equivalent RLC Circuit of Network

For the analysis, the FB-MMC-based bipolar 5-terminal DC network is under study. The single-line diagram of the proposed test system having each MMC station connected to the AC source is shown in Fig.2. Table I lists the operating conditions and MMC parameters of each station, while Table II demonstrates the specifications of the DC distribution lines.

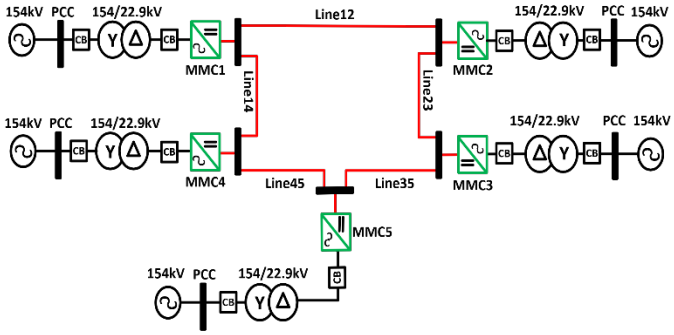

Fig. 2 Five Terminal Bipolar MMC-based MTDC Network

The equivalent RLC model of the test system is shown in Fig.3 under normal operation. The subscripts e_{ip} and e_{in} show the positive and negative MMC equivalent parameters respectively, where *i=1,2,3,4....* u_{c_p} and u_{c_n} denote the equivalent voltages across positive and negative nodes of MMC. The red line denotes the branch equivalent, and the black indicates the MMC equivalent.

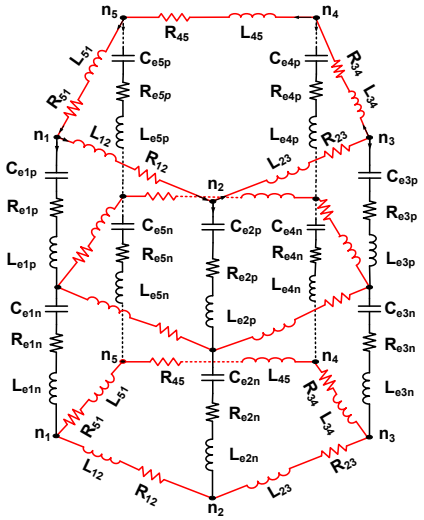

Fig. 3 Equivalent RLC Model for Bipolar 5-Terminal MTDC Network

III. MATHEMATICAL MODELING OF FAULT CURRENT FOR DC SYSTEM

There are two distinct phases to the fault current that passes through the MMC: before MMC blocking and after MMC blocking. Without considering blocking, we may examine the fault current behavior in the MMC in three stages to better understand it. The submodule (SM) capacitors must be discharged in the first step (I). In the second stage (II), inductor discharge, SM capacitor-discharge, and AC grid feeding are all combined. In the third stage (III), only AC grid feeding is used. Fig.4 illustrates these steps.

TABLE I MMC PARAMETERS FOR MTDC NETWORK

Stations	L_{SM} (H)	C_{SM} (F)	Capacity	Control Mode
MMC1	0.0039	0.0200	20kV	Voltage
MMC2	0.0026	0.0300	-40MW	Power
MMC3	0.0103	0.0075	10MW	Power
MMC4	0.0103	0.0075	-10MW	Power
MMC5	0.0103	0.0075	10MW	Power

TABLE II SYSTEM RATING AND LINE PARAMETERS IN MTDC NETWORK

Parameters	Rating
Rated DC Voltage (kV)	20
Transformer voltage ratio (kV/kV)	154/22.9
Per unit Length Resistance (Ω/Km)	0.1×10^{-3}
Number of Sub-Modules (N_{SM})	20
Per unit Length Inductance (mH/Km)	0.02×10^{-3}
Smooth Reactor DC	2×10^{-3}

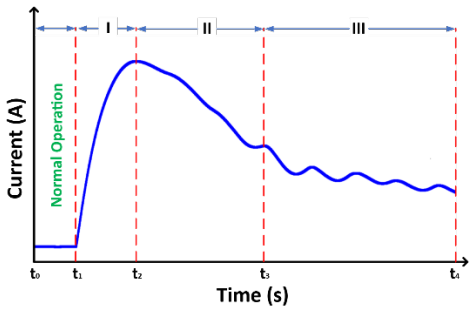

Fig. 4 Fault Current Stages in MMC

The SM capacitors discharge into the system when a fault arises. The primary source of the peak fault current in the first stage is the discharge current from the capacitor. This early phase of the MMC action before blocking is the focus of our investigation.

For a, *b* branches and *n* node in MMC-based DC circuits, the branch current *i*, node voltage *u,* and the injection current by the MMC i_c are defined in matrix form as

$$i = [\, i_{12} \dots \dots . i_{ij} \dots \dots \dots]^T{}_b \quad (9)$$

$$u = [\, u_{c1}\, u_{c2} \dots . . \dots . u_{cN}]^T{}_n \quad (10)$$

$$i_c = [\, i_{c1}\ i_{c2}\ \dots . \dots \dots . i_{cn}]^T{}_n \quad (11)$$

Source current vector $i_s = [i_{s1} \dots\dots i_{si} \dots]^T$ and branch current can be calculated using the dynamic equation given in (12). This is a general equation for the MTDC system, it can be modified according to the network structure. In the equation matrix *L* and *R* are the inductance and resistance matrix of the DC network and *A* is the incidence. The starting and ending of the branches between nodes are determined in [25];

$$aki = \begin{cases} 1, & if\ node\ is\ starting\ point \\ -1, & if\ node\ is\ ending\ point \\ 0, & otherwise \end{cases}$$

$$A.u = R.i + L\frac{di}{dt} \quad (12)$$

The relationship between inserted current $\boldsymbol{i_c}$ and the branch current $\boldsymbol{i}$ is shown as follows

$$i_c = -A^T.i \quad (13)$$

A. Pole-to-pole Fault

When a PTP fault occurs in a system, it distributes the fault branch into two, thus the incidence matrix *A*, resistance matrix *R*, and inductance matrix *L* should include the fault branch for the accurate calculation. Suppose a fault occurs in the ij branch at the fault node n_0, the branch is divided into two new branches i_0 and j_0, the PTP fault equivalent circuit is shown in Fig. 5.

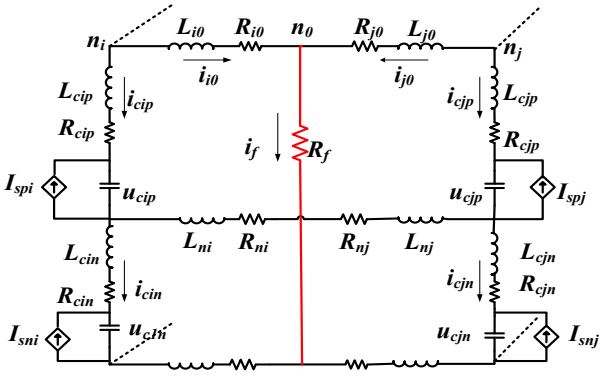

Fig. 5 Fault Branch Equivalent Model for MTDC network

For the PTP fault branch resistance is divided into R_{i0} and R_{j0}. Similarly, the branch inductance is L_{i0} and L_{j0} and the current is i_{i0} and i_{j0} respectively. The fault resistance is denoted by R_f. Modified branch current matrix *i* shown in (14)

$$i = [\, i_{12} \dots \dots . i_{i0}\ i_{j0} \dots \dots \dots]^T{}_{b+1} \quad (14)$$

Meanwhile, the inductance metric and resistance metric are modified into two rows and two columns, and the dimension of A is changed from *b* x *n* to *(b+1)* x *n*.

In a bipolar, two MMCs are connected in the cascaded structure and the midpoint is connected to the neutral line. For a PTP fault that occurs in the bipolar system, the branch current in a positive terminal and negative terminal are the same and their system behaviors are like the monopole structure because no current is flowing through the neutral line. Thus, for the bipolar system, the dynamic equation is modified, and a new equation is given as (15)

$$A.(u_p + u_n) = R.i + L\frac{di}{dt} \quad (15)$$

Where the subscript *p* and *n* denote the positive and negative poles of MMC. The relation between the branch current and the incidence current $i_{cp,n}$ for the bipolar structure is

$$i_{cp,n} = -A^T.i \quad (16)$$

Thus, it is possible to determine the relationship between the node voltages, branch currents, and source currents.

$$\frac{d}{dt}u_{cp,n} = K(i_{cp,n} + i_{sp,n}) \quad (17)$$

And $K = diag\left[\frac{1}{C_{e1\,p,n}} \dots \dots \dots \dots \dots \frac{1}{C_{ei\,p,n}}\right]$

The following conditions are considered when determining matrix *R* and *L*:

- All the resistances in a branch equation's path are contained in each diagonal element in *R* and *L*.
- A non-diagonal element of branch *ij* shows the resistance through which other branch current passes.
- The branch current's reference direction determines the sign of each non-diagonal element.

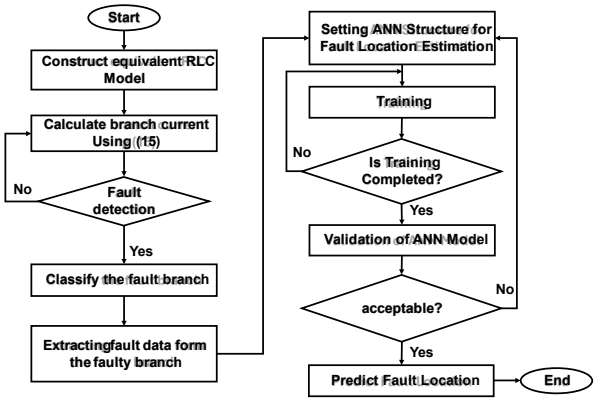

Fig. 6 Flow Chart of the proposed algorithm

The branch currents and the node voltage for a PTP fault in the

bipolar MTDC network can be obtained accurately using (15) and (17).

IV. Fault Current Calculation and Fault Location Estimation

The current of the faulty branch serves as a critical parameter for extracting data, which is subsequently utilized in developing algorithms for both fault line detection and fault location estimation. The flowchart presented in Fig.6 outlines the entire process, starting from the branch current calculation to the implementation of fault location estimation algorithms.

A. Fault Current Calculation

A thorough examination of fault currents in the Multi-Terminal DC (MTDC) network is carried out to enable precise fault location estimation. A 5-terminal MTDC network with a 40kV voltage rating serves as the test system for this investigation shown in Fig. 2. To analyze the system's response and determine the resulting fault currents across each branch, a PTP fault is introduced on line 12. MATLAB is used to calculate fault current and voltage by solving the differential equations (15) and (17) using ordinary differential equations for various points along a branch with different fault resistances R_f to acquire PTP fault current data. The total length of the distribution line between two adjacent nodes is 30 km. Table III demonstrates the range of the fault resistance taken and the line length division to extract fault data. For the fault on line 12 the incidence matrix A, resistance matrix R, and inductance matrix L are given in the Appendix.

$$A = \begin{bmatrix} 1 & 0 & 0 & 0 & 0 \\ 0 & -1 & 0 & 0 & 0 \\ 0 & 1 & -1 & 0 & 0 \\ 0 & 0 & 1 & -1 & 0 \\ 0 & 0 & 0 & 1 & -1 \\ -1 & 0 & 0 & 0 & 1 \end{bmatrix} \quad (18)$$

Branch current vector i and node voltage u for the PTP fault that occurs in the system can be defined as

$$i = [i_{12},\ i_{20}, i_{03},\ i_{34}, i_{45}, i_{51}]$$
$$u = [u_1,\ u_2, u_3, u_4, u_5]$$

Where, $u_i = u_{ip} + u_{in}$ *and* $i = 1,2,3,4 \ldots\ldots$

TABLE III VARIABLE FAULT LENTH AND FAULT RESISTANCE

Parameter	Range	Division
Line Length (L)	0-30km	0.200km
Fault Resistance (R_f)	0-10 Ω	0.25 Ω

Fig.7 shows the calculated fault current for three different fault resistance R_f, for the same time and same fault location. From the result, it can be noticed that if the fault resistance is increased the magnitude of the fault current decreases dramatically, while Fig.8 shows the fault current at different locations with constant R_f, resulting in a decrease of the fault current but in compression to the fault resistance effect, it shows a small impact on fault magnitude.

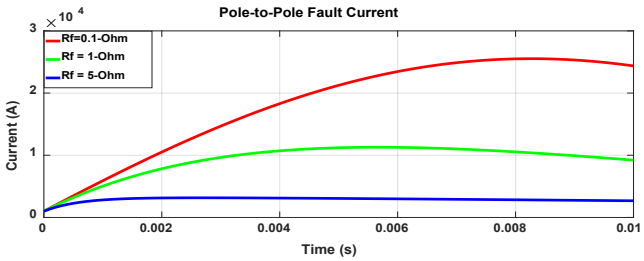

Fig. 7 Fault Current Behavior Under Variable Fault Resistances

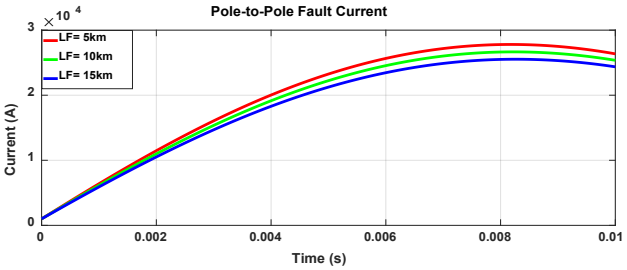

Fig. 8 Fault Current Behavior for Different Fault Locations

B. Fault Line Detection

For fault line detection the branch currents under fault conditions are used. If a fault occurs on the branch, the current flowing through the line increases abruptly, this change in branch current is used to detect the faulty line in the network.

C. Fault Location Estimation Algorithm

For MVDC systems to be more reliable and have shorter restoration times, precise fault location is essential, particularly in bipolar multi-terminal DC (MTDC) networks. The fault current data is obtained from mathematical models of the MTDC network under various fault situations to train an ANN-based fault location estimation algorithm. The goal of the method is to accurately locate the fault in the network while considering a variety of fault locations and fault resistances. The design, training process, and algorithm's ability to precisely locate PTP faults are described in this section.

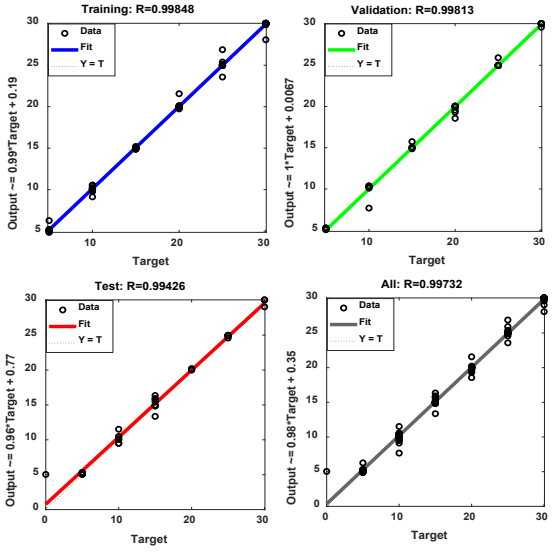

Fig. 9 ANN Model Fault Location Estimation Training, validation, and Testing results

Fig.9 presents regression plots evaluating the proposed ANN model for fault location estimation in a 5-terminal MTDC network. The results show a near-perfect correlation between predicted and target values in the training phase. The fit equation shows a nearly perfect connection between the predicted and target values during the training phase, as indicated by the regression coefficient R = 0.9984. The output is within the range of 0.99 × Target + 0.19. Similarly, the validation dataset shows an excellent correlation with R = 0.99813 when the parameters are tuned. Moreover, the model works well when applied to test data that is not visible, demonstrating its dependability and resilience. Based on the model's overall performance, integrating all datasets, fault location is reliably and consistently estimated.

The ANN algorithm performance for fault location estimation in a 5-terminal MTDC system is depicted in Fig.10. The actual fault location is displayed on the y-axis, while the x-axis represents fault cases. The blue solid line indicates the actual fault location, while the predicted red dashed line represents fault locations predicted by ANN. The close alignment of the two lines suggests the precision of the ANN in determining the fault location with minimal deviation from the actual values, demonstrating its accuracy and reliability in fault location estimation.

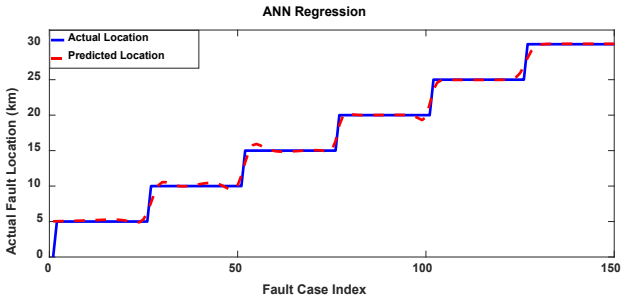

Fig. 10 ANN Regression Model Output

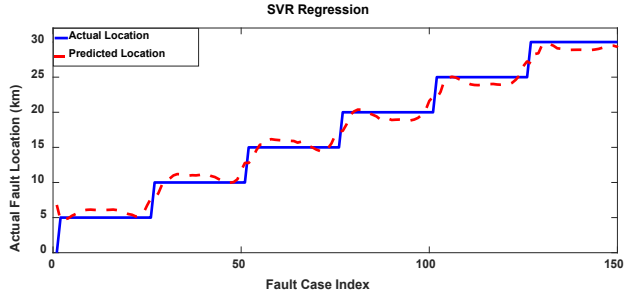

Fig. 11 SVR Regression Model Output

D. Performance analysis of the proposed algorithm

To evaluate the performance of the model, and ensure its effectiveness, the model is compared to the existing SVR model to demonstrate its exceptional precision and dependability. Fig.11 illustrates the SVR regression performance.

The following three important metrics were used to examine the effectiveness of the ANN and SVR models for fault location estimation in the bipolar medium voltage MTDC network: Root Mean Square Error (RMSE), Mean Absolute Error (MAE), and Coefficient of Determination (R^2). Table IV provides a summary of the outcomes of various indicators.

TABLE IV PERFORMANCE METRICS COMPARISON

Metric	ANN	SVR
RMSE	0.8090	1.2209
MAE	0.3896	0.9525
R^2	0.9912	0.9800

Across all assessed performance measures, the ANN model performs better than the SVR model. For fault location estimation in the MTDC network, its better R^2 value and reduced error rates (RMSE and MAE) demonstrate its exceptional precision and dependability. While the SVR model yields results, it is less capable of managing the non-linearities present in fault scenarios, that is why ANN is recommended to precisely estimate fault locations.

The outcomes of the ANN algorithm with mathematical modeling demonstration to pinpoint fault location with reduced percentage error. The model's capacity to generalize effectively and precisely estimate fault locations across a range of circumstances is demonstrated by the high R-values for each phase. Table V shows compression with existing schemes.

TABLE V COMPRESSION WITH EXISTING METHODS

FL- Method	Converter	Methodology	Configuration	Accuracy /Time
Traveling wave [20]	Monopole	Simulation	MT-HVDC	80ms
Artificial intelligence [22]	Voltage-Source Converters (VSC)	Simulation	MT-HVDC	97.5%
Inductance-based [26]	VSC	Simulation and HIL	Point-to-Point and MTDC	N/A
Voltage ratio-based [27]	VSC	Simulation and HIL.	MT-MVDC	1.5ms
Proposed ANN	Bipolar FB-MMC	Analytical Equation-Based	MT-MVDC	99.12%

E. Performance Analysis of ANN on Non-Ideal Condition

Real-world power systems will inevitably have measurements and sensor noise. To evaluate the algorithm's performance in noisy environments, an additive white Gaussian noise (AWGN) at three distinct signal-to-noise ratio (SNR) levels are introduced. As indicated in Table VI, the classification performance was assessed using the RMSE, MAE, and R^2 metrics. The findings show that the model retains an R^2 over 0.97, demonstrating its robustness, even when increasing noise reduces accuracy.

TABLE VI PERFORMANCE METRICS WITH NOISE

Noise Level(db)	RMSE	MAE	R^2
20db	1.4129	0.7912	0.9732
40db	1.1948	0.7586	0.9808
60db	0.8527	0.5805	0.9902
No noise	0.8090	0.3896	0.9912

Variations in temperature, aging, or manufacturing tolerances can affect distribution line parameters like resistance

(R_{dc}) and inductance (L_{dc}). Deviations of ±10% and ±20% from the nominal values are considered and examined the impact on performance to evaluate the robustness of the suggested fault classification technique.

The RMSE, MAE, and R^2 metrics for various parameter modifications are shown in Table VII. As the R^2 stays over 0.98, the data show that variation has no effect on accuracy. This implies that the model is very resistant to changes in the parameters of the transmission line.

TABLE VII PERFORMANCE METRICS WITH LINE PARAMETERS

Variation in (R_{dc} and L_{dc})	RMSE	MAE	R^2
-20%	0.8782	0.6155	0.9896
-10%	0.8532	0.6041	0.9902
Nominal	0.8090	0.3896	0.9912
10%	0.8734	0.6144	0.9898
20%	0.8824	0.6204	0.9895

In DC transmission systems, power converters play a crucial role in fault identification and categorization. However, factors such as production tolerances, environmental conditions, and component aging can impact their performance. To evaluate the proposed algorithm's resilience in less-than-ideal conditions, various converter parameters were adjusted, including submodule resistance (R_0), inductance (L_0), capacitance (C_0), and the proportional (K_p) and integral (K_i) control gains of the converter controller. Table VIII summarizes the effect of these adjustments on the algorithm's performance, showing that the model maintains an R^2 value over 0.97, demonstrating its robustness.

TABLE VIII VARIATION IN CONVERTER PARAMETERS

Variation in Converter Parameters	RMSE	MAE	R^2
-20% (R_0, L_0 and C_0)	0.8747	0.6163	0.9897
20% (R_0, L_0 and C_0)	0.8677	0.6142	0.9899
-20% (Kp, Ki)	1.2547	0.9987	0.9789
20% (Kp, Ki)	1.2878	1.0150	0.9777

The proposed algorithm is tested for various non-ideal conditions under noise-added data, line parameters, and converter parameter variations to simulate real-world scenarios. However, since the study is based on simulation-generated data, its performance in actual MVDC networks may vary. Future work will focus on hardware-in-the-loop (HIL) testing to further validate its practical applicability and robustness.

V. CONCLUSIONS

This work focuses on PTP faults and provides a robust method for calculating faults and estimating their locations in the MTDC distribution system. An ANN algorithm is trained with this extensive dataset to precisely detect fault locations by using mathematical modeling to extract fault current data under different fault locations and fault resistances. The datasets are divided into 80% of the data used for training, 10% for validation, and 10% for testing. The system shows consistent performance in accurately estimating fault location.

The results highlight how the ANN algorithm combined with mathematical modeling can improve the MVDC network's fault detection and localization capabilities. The results demonstrate that the ANN-based fault location approach achieves high accuracy, with an RMSE of 0.8090 and R^2 of 0.9912, outperforming SVR, which achieves an RMSE of 1.2209 and R^2 of 0.9800. Further analysis, including the presence of noise and parameter deviations in transmission lines and converters, confirms the robustness of the method. The ANN maintains a high R^2 above 0.97, even with noise and variations in system parameters, demonstrating its reliability in practical applications.

This method provides substantial advantages for MVDC system safety, enabling faster fault diagnosis, reduced restoration time, and improved system dependability. Modern DC distribution networks that increasingly use RES can benefit from the scalable and flexible solution offered by the suggested approach, which can be incorporated into current MVDC protection programs. Future studies should investigate real-time implementation and extend this approach to other fault types to improve the operational efficiency and resilience of MVDC networks.

VI. APPENDIX

$$R = \begin{bmatrix} R_{e1} + 2R_{10} + R_f & -R_f & 0 & 0 & 0 & -R_{e1} \\ -R_f & R_f + 2R_{20} + R_{e2} & -R_{e2} & 0 & 0 & 0 \\ 0 & -R_{e2} & R_{e2} + 2R_{23} + R_{e3} & -R_{e3} & 0 & 0 \\ 0 & 0 & -R_{e3} & R_{e3} + 2R_{34} + Re4 & -R_{e4} & 0 \\ 0 & 0 & 0 & -R_{e4} & R_{e4} + 2R_{45} + R_{e5} & -R_{e5} \\ -R_{e1} & 0 & 0 & 0 & -R_{e5} & R_{e5} + 2R_{51} + R_{e1} \end{bmatrix}$$

$$L = \begin{bmatrix} L_{e1} + 2L_{10} & 0 & 0 & 0 & 0 & -L_{e1} \\ 0 & L_{e2} + 2L_{20} & -L_{e2} & 0 & 0 & 0 \\ 0 & -L_{e2} & L_{e2} + 2L_{23} + L_{e3} & -L_{e3} & 0 & 0 \\ 0 & 0 & -L_{e3} & L_{e3} + 2L_{34} + L_{e4} & -L_{e4} & 0 \\ 0 & 0 & 0 & -L_{e4} & L_{e4} + 2L_{45} + L_{e5} & -L_{e5} \\ -L_{e1} & 0 & 0 & 0 & -L_{e5} & L_{e5} + 2L_{51} + L_{e1} \end{bmatrix}$$

VII. ACKNOWLEDGMENT

The authors gratefully acknowledge the contributions of A.Mehdi, G.Shin, S.J.Hassan, and C.H.Kim for their work on the original version of this document.

VIII. REFERENCES

[1] D. Gielen, F. Boshell, D. Saygin, M. D. Bazilian, N. Wagner, and R. Gorini, "The role of renewable energy in the global energy transformation," *Energy Strategy Reviews*, vol. 24, pp. 38–50, Apr. 2019, doi: 10.1016/j.esr.2019.01.006.

[2] S. J. U. Hassan *et al.*, "Towards medium voltage hybrid AC/DC distribution Systems: Architectural Topologies, planning and operation," Aug. 01, 2024, *Elsevier Ltd*. doi: 10.1016/j.ijepes.2024.110003.

[3] M. Shafiul Alam, F. S. Al-Ismail, A. Salem, and M. A. Abido, "High-level penetration of renewable energy sources into grid utility: Challenges and solutions," *IEEE Access*, vol. 8, pp. 190277–190299, 2020, doi: 10.1109/ACCESS.2020.3031481.

[4] L. Zhang, L. Harnefors, and H. P. Nee, "Power-synchronization control of grid-connected voltage-source converters," *IEEE Transactions on Power Systems*, vol. 25, no. 2, pp. 809–820, May 2010, doi: 10.1109/TPWRS.2009.2032231.

[5] A. Mehdi, S. J. Ul Hassan, Z. Haider, A. D. Arefaynie, J. sol Song, and C. H. Kim, "A systematic review of fault characteristics and protection schemes in hybrid AC/DC networks: Challenges and future directions," Dec. 01, 2024, *Elsevier Ltd*. doi: 10.1016/j.egyr.2024.05.077.

[6] C. Li, C. Zhao, J. Xu, Y. Ji, F. Zhang, and T. An, "A Pole-to-Pole Short-Circuit Fault Current Calculation Method for DC Grids," *IEEE Transactions on Power Systems*, vol. 32, no. 6, pp. 4943–4953, Nov. 2017, doi: 10.1109/TPWRS.2017.2682110.

[7] Marco Stieneker and Rik W. De Doncker, "Medium-voltage DC distribution grids in urban areas," in *2016 IEEE 7th International Symposium on Power Electronics for Distributed Generation Systems (PEDG)*, IEEE, 2016. doi: 10.1109/PEDG.2016.7527045.

[8] Q. Qi, C. Long, J. Wu, and J. Yu, "Impacts of a medium voltage direct current link on the performance of electrical distribution networks," *Appl Energy*, vol. 230, pp. 175–188, Nov. 2018, doi: 10.1016/j.apenergy.2018.08.077.

[9] Z. Ali *et al.*, "Fault Management in DC Microgrids: A Review of Challenges, Countermeasures, and Future Research Trends," *IEEE Access*, vol. 9, pp. 128032–128054, 2021, doi: 10.1109/ACCESS.2021.3112383.

[10] M. Langwasser, G. De Carne, M. Liserre, and M. Biskoping, "Fault current estimation in multi-terminal hvdc grids considering mmc control," *IEEE Transactions on Power Systems*, vol. 34, no. 3, pp. 2179–2189, May 2019, doi: 10.1109/TPWRS.2018.2887166.

[11] Q. Liu, P. Sun, S. Jiang, F. Arraño-Vargas, and G. Konstantinou, "Calculation of DC Fault Current and Analysis of Influencing Factors in MMC-based Medium Voltage DC Systems," in *2023 IEEE International Conference on Energy Technologies for Future Grids, ETFG 2023*, Institute of Electrical and Electronics Engineers Inc., 2023. doi: 10.1109/ETFG55873.2023.10408381.

[12] P. Huang, S. Shah, and L. Vanfretti, "Active Fault Current Limiting Control for Half-bridge MMC in HVDC Systems," in *2023 IEEE 24th Workshop on Control and Modeling for Power Electronics, COMPEL 2023*, Institute of Electrical and Electronics Engineers Inc., 2023. doi: 10.1109/COMPEL52896.2023.10221028.

[13] G. W. Kim and H. S. Choi, "Limiting Characteristics of Capacitor Discharge Current of MMC-Based System Using the SFCL on Short Circuit," *IEEE Transactions on Applied Superconductivity*, vol. 32, no. 4, Jun. 2022, doi: 10.1109/TASC.2022.3140697.

[14] P. Wang, M. Kuschke, and K. Strunz, "Analytical Modeling of Modular Multilevel Converter Under Pole-to-Pole DC Fault and Application to System Design and Protection," *IEEE Transactions on Energy Conversion*, vol. 37, no. 4, pp. 2722–2736, Dec. 2022, doi: 10.1109/TEC.2022.3209553.

[15] Simon Beckler, Joachim Lehner, Akos Arnold, Alain Kaptue Kamga, Katharina Frey, and Krzysztof Rudion, "DC Fault Currents for FB-MMC HVDC with Bipolar Configuration," in *International ETG Congress 2015; Die Energiewende - Blueprints for the new energy age*, VDE, 2016.

[16] S. Gao, H. Ye, and Y. Liu, "Accurate and Efficient Estimation of Short-Circuit Current for MTDC Grids Considering MMC Control," *IEEE Transactions on Power Delivery*, vol. 35, no. 3, pp. 1541–1552, Jun. 2020, doi: 10.1109/TPWRD.2019.2946603.

[17] H. Ye, S. Gao, G. Li, and Y. Liu, "Efficient Estimation and Characteristic Analysis of Short-Circuit Currents for MMC-MTDC Grids," *IEEE Transactions on Industrial Electronics*, vol. 68, no. 1, pp. 258–269, Jan. 2021, doi: 10.1109/TIE.2020.2965433.

[18] Y. Xu *et al.*, "A Practical Pole-to-Ground Fault Current Calculation Method for Symmetrical Monopole DC Grids," *Electronics (Switzerland)*, vol. 13, no. 21, Nov. 2024, doi: 10.3390/electronics13214245.

[19] H. Sun, K. Ammann, S. Giannoulakis, and O. Fink, "Continuous Test-time Domain Adaptation for Efficient Fault Detection under Evolving Operating Conditions," Jun. 2024, [Online]. Available: http://arxiv.org/abs/2406.06607

[20] S. Azizi, M. Sanaye-Pasand, M. Abedini, and A. Hassani, "A traveling-wave-based methodology for wide-area fault location in multiterminal DC systems," *IEEE Transactions on Power Delivery*, vol. 29, no. 6, pp. 2552–2560, Dec. 2014, doi: 10.1109/TPWRD.2014.2323356.

[21] K. Jia, T. Bi, Z. Ren, D. W. P. Thomas, and M. Sumner, "High frequency impedance based fault location in distribution system with DGs," *IEEE Trans Smart Grid*, vol. 9, no. 2, pp. 807–816, 2018, doi: 10.1109/TSG.2016.2566673.

[22] A. Hossam-Eldin, A. Lotfy, M. Elgamal, and M. Ebeed, "Artificial intelligence-based short-circuit fault identifier for MT-HVDC systems," *IET Generation, Transmission and Distribution*, vol. 12, no. 10, pp. 2436–2443, May 2018, doi: 10.1049/iet-gtd.2017.1345.

[23] M. Egan, J. Thapa, and M. Benidris, "Machine Learning Using High-Precision Data for Fault Location," in *2022 17th International Conference on Probabilistic Methods Applied to Power Systems, PMAPS 2022*, Institute of Electrical and Electronics Engineers Inc., 2022. doi: 10.1109/PMAPS53380.2022.9810580.

[24] Y. Yuan, J. Li, P. Lyu, Z. Qian, Y. Jiang, and J. Wang, "Modified Fault Current Calculation Scheme Combined with MMC Control for AC/DC Distribution Networks," *IEEE Access*, vol. 12, pp. 106822–106831, 2024, doi: 10.1109/ACCESS.2024.3436667.

[25] M. Langwasser, G. De Carne, M. Liserre, and T. Schindler, "Requirement analysis of hybrid direct current breaker in multi-terminal high-voltage direct current grids," *The Journal of Engineering*, vol. 2018, no. 15, pp. 1066–1071, Oct. 2018, doi: 10.1049/joe.2018.0267.

[26] D. Li and A. Ukil, "Fault Location Estimation in Voltage-Source-Converter-Based DC System: The L Location," *IEEE Transactions on Industrial Electronics*, vol. 69, no. 11, pp. 11198–11209, Nov. 2022, doi: 10.1109/TIE.2021.3125662.

[27] Y. Yang and C. Huang, "DC fault location in multi-terminal DC distribution network based on voltage similar triangle principle," *Electric Power Systems Research*, vol. 184, Jul. 2020, doi: 10.1016/j.epsr.2020.106306.